Progress In Electromagnetics Research C, Vol. 116, 181–192, 2021

A Dual-Beam Switchable Self-Oscillating Ku-Band Active Array Antenna Integrating Positive Feedback Type Push-Push Oscillator and PSK Modulator

Maodudul Hasan*, Eisuke Nishiyama, Takayuki Tanaka, and Ichihiko Toyoda

Abstract—This paper proposes a dual-beam switchable self-oscillating active integrated array antenna for Ku-band wireless power transfer systems. The oscillation is sourced by a positive feedback type Push-Push oscillator, which shows an excellent measured output power of +9.3 dBm obtained at the second harmonic frequency as well as good suppression of the undesired harmonics. The generated RF power from the oscillator excites four patch antenna elements. Moreover, a PSK modulator is adopted for binary phase switching between 0° and 180°. Using in/anti-phase RF signal combination of the antenna elements, it is possible to switch between two beams, sum and difference radiation patterns. The proposed structure is fabricated and tested; the measured results verify the dual-beam switching concept with an effective isotropic radiated power (EIRP) of +17.77 dBm, DC-to-RF efficiency of 0.43%, and an oscillator figure of merit (FOM) of −158.05 dBc/Hz at the second harmonic frequency of 14.7 GHz.

1. INTRODUCTION

Active integrated antennas (AIAs) have prominent features that make them attractive in millimeter-wave systems featuring low transmission-line loss, compactness, and low cost [1, 2]. Microstrip antennas integrated with an oscillator or directly connected with active devices form an active oscillating type AIA. In an oscillating type microwave and millimeter-wave AIA, high performance, low phase noise, and low-cost sources are essential. However, highly stable high-frequency sources with good output power are a challenging task. In general, two and three-terminal devices, mainly Gunn diodes [3–7] and FETs [8, 9, 11–18] are used as an active device. But at high frequency, power handling capability of those devices decreases. Push-Push oscillators are considered as one of the effective techniques to extend the frequency range of the active devices [19].

Several AIAs have already been reported in [8–18]. In [18], a Push-Push oscillator, PSK modulator, and ring-slot array antenna have been studied separately to propose a concept of self-oscillating active integrated array antenna (AIAA) for transmitter module. Nowadays, integration approach becomes matured, and therefore, many reconfigurable AIAAs including polarization [3–6], frequency [17], and pattern [8–10] functions have been reported in the literature. Besides, beam switchable AIAAs [7, 12–14] have also been studied as they have multi-directive beams to resolve multi-path and interference effects by redirecting their radiation patterns [20].

In this study, we proposes a 2×2 array antenna integrated with a positive feedback type Push-Push oscillator and PSK modulator to attain self-oscillating capability and dual-beam switching functionality for Ku-band applications following our previous paper [16]. This AIA can be used in Radio Frequency Identification (RFID) systems, wireless power transfer (WPT) systems, indoor wireless positioning systems, and Doppler transceivers.

Received 28 September 2021, Accepted 1 November 2021, Scheduled 8 November 2021

* Corresponding author: Maodudul Hasan (hasan@ceng.ec.saga-u.ac.jp).

The authors are with the Department of Electrical and Electronic Engineering, Saga University, 1 Honjo-machi, Saga-shi, Saga

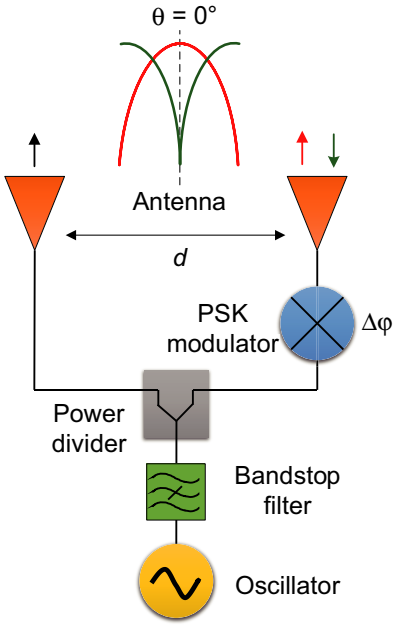

Figure 1. Block diagram of the proposed dual-beam switchable AIAA.

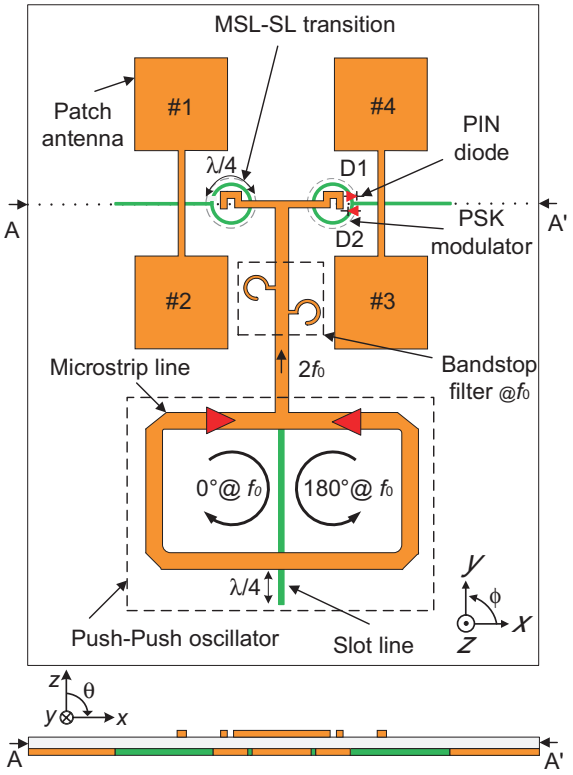

Figure 2. Circuit layout of the proposed dual-beam switchable self-oscillating AIAA.

2. DESIGN OF BEAM SWITCHABLE AIAA

2.1. AIAA Configuration

Figure 1 shows the block diagram of the proposed dual-beam switchable AIAA's concept. The proposed beam switchable antenna consists of two sets of antennas, an oscillator, a bandstop filter, a power divider, and a PSK modulator. The oscillator generates radio frequency (RF) signal that passes through the bandstop filter. A T-type power divider circuit is attached to the proposed antenna to split the generated RF power to feed the two sets of the antenna elements. The PSK modulator is used to alter the input signal's phase fed to either one of the two sets of the antenna elements. Therefore, the antenna elements are excited with either in- or anti-phase signal. Thus, the power combination of the electric fields from the antenna elements generate either sum or difference radiation pattern. In the proposed antenna, the PSK modulator controls the radiation pattern. The principle of this dual-beam switching can be explained by using the array factor. For N elements of uniformly spaced linear arrays, the array factor can be expressed as follows [23]:

$$AF(\theta, \Delta\varphi) = \frac{\sin\left[N\left(\frac{\pi d}{\lambda}\sin\theta - \frac{\Delta\varphi}{2}\right)\right]}{N\sin\left[\left(\frac{\pi d}{\lambda}\sin\theta - \frac{\Delta\varphi}{2}\right)\right]}. \quad (1)$$

where θ, $\Delta\varphi$, and d are the beam angle, phase shift between the elements, and patch spacing, respectively. If the phase difference $\Delta\varphi$ is 0°, Eq. (1) provides the sum pattern. In contrast, the difference pattern can be found for 180° phase shift between the elements. The peak can be determined

840-8502, Japan.

by the equation below,

$$\theta = \pm \sin^{-1}\left(\frac{\lambda}{2d}\right). \tag{2}$$

when each antenna element is isotropic.

Figure 2 illustrates the schematic layout of the proposed dual-beam switchable AIAA. Four antennas are equally spaced to achieve a high gain. The antenna elements #1, #2 and #3, #4 form two sets of antennas. The phases of the antenna elements #3 and #4 can be altered through the PSK modulator, whereas the phases of the antenna elements #1 and #2 are constant. The PSK modulator has two PIN diodes, D1 and D2 to control the phase switching of the fed signal. To achieve symmetrical configuration, a microstrip-slot (MSL-SL) transition is designed like the PSK modulator geometry. The generated RF power of the positive feedback type Push-Push oscillator is fed to the antenna elements through the feeding circuit including a bandstop filter.

2.2. Push-Push Oscillator

Figure 3 shows the block diagram of the positive feedback type Push-Push oscillator. It consists of two identical feedback loops. The oscillation frequency is determined by the electrical length of the feedback loops. Due to the magic-T, only the fundamental and odd harmonic signals go back to the loops, and even harmonics emerge at the output port.

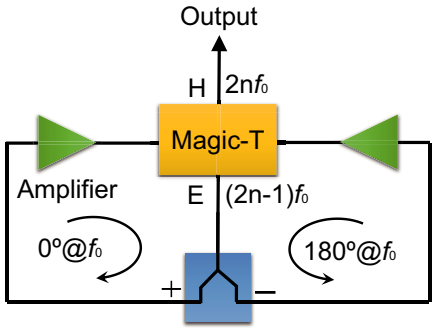

Figure 3. Block diagram of the positive feedback type Push-Push oscillator used in the proposed AIAA.

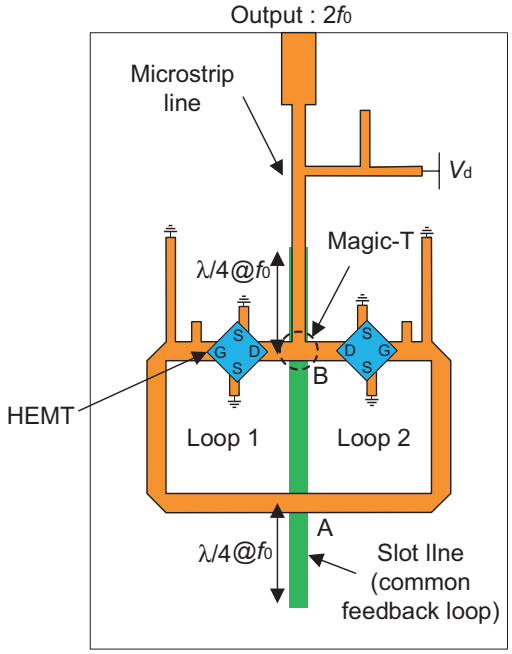

Figure 4. Structure of the positive feedback type Push-Push oscillator.

Figure 4 shows the circuit structure of the positive feedback type Push-Push oscillator [21] used in the proposed AIAA. The Push-Push oscillator consists of two amplifiers using HEMTs as an active device and a common biasing circuit. Here, the yellowish and green lines represent the microstrip and slot line, respectively. The slot line is very important for the operation of this Push-Push oscillator. It acts as a common feedback loop. Moreover, it also creates a slot-microstrip power divider and magic-T referring to point A and B, respectively.

Figure 5 explains the operational mechanism of points A and B of Fig. 4. Fig. 5(a) illustrates the slot-microstrip power divider of point A. The input signal from the slot line is equally divided but into

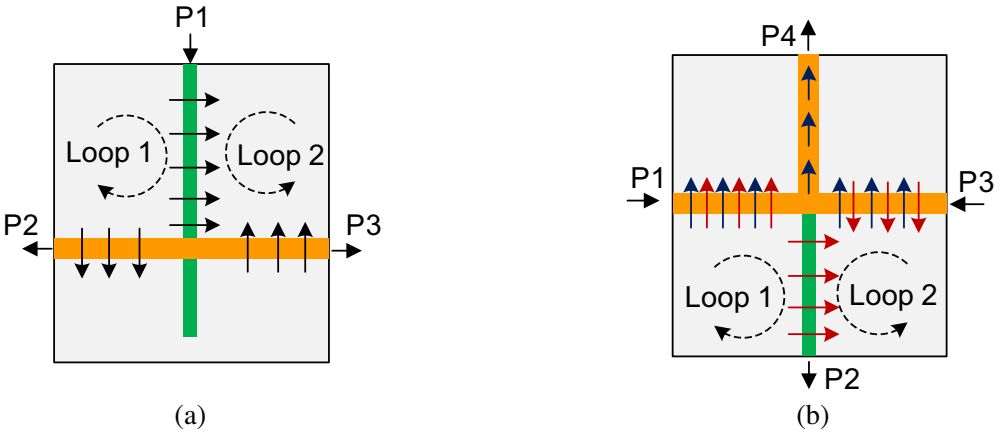

Figure 5. Operational mechanism of point A and B of Fig. 4. (a) Slot-microstrip power divider, point A. (b) Magic-T, point B.

anti-phase due to the balanced mode of the slot line at the slot-microstrip power divider. Thus 180° phase difference is realized between the two loops at the fundamental frequency. The oscillation signals of the feedback loops in the Push-Push oscillator, V_{osc1} and V_{osc2}, can be written as

$$V_{\text{osc1}} = \sum_n a_n e^{jn\omega_0 t} \tag{3}$$

$$V_{\text{osc2}} = \sum_n a_n e^{jn(\omega_0 t+\pi)}. \tag{4}$$

Here, a_n, ω_0, and n represent the amplitude, angular frequency of the fundamental signal, and harmonic index, respectively.

Figure 5(b) shows point B of Fig. 4, which is a planar magic-T. Here, the red and blue arrowhead lines pertain to the anti-phase and in-phase signals, respectively. When two anti-phase signals are fed from ports P1 and P3, they are combined and feed back to point A through port P2 of the magic-T. On the other hand, the even harmonics are combined and emerge at the output port P4. Thus, the output signal of the Push-Push oscillator is expressed as follows:

$$V_{\text{out}} = V_{\text{osc1}} + V_{\text{osc2}} = 2a_2 e^{j2\omega_0 t} + 2a_4 e^{j4\omega_0 t} + 2a_6 e^{j6\omega_0 t} + \ldots \tag{5}$$

Figure 6 shows the simulated output power of the proposed Push-Push oscillator. The oscillator is designed for the fundamental frequency of 8 GHz. Better than +7.7 dBm output power is shown at the second harmonic frequency following the Eq. (5), and thus, it confirms the Push-Push operational theory.

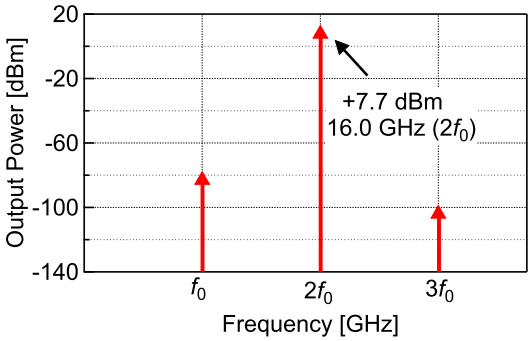

Figure 6. Simulated output power of the Push-Push oscillator.

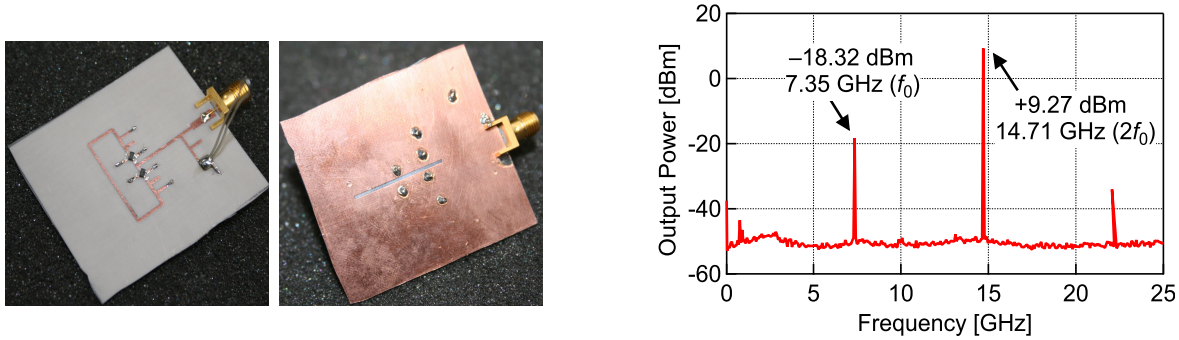

Figure 7. Fabricated prototype and measured result of the Push-Push oscillator. (a) Photograph of the prototype Ku-band oscillator (50 mm × 45 mm). (b) Measured output power at 5-V, 230-mA bias condition.

Figure 7(a) shows a photograph of the fabricated Ku-band positive feedback type Push-Push oscillator, and the size of the oscillator is 50 mm × 45 mm. The utilized HEMT transistors in this design are ATF34143 manufactured by Avago. Fig. 7(b) shows the measured output power using a spectrum analyzer Agilent E4407B. An excellent output power of +9.3 dBm is obtained at the second harmonic frequency of 14.71 GHz. Moreover, the result shows a good 27-dB suppression of the unwanted fundamental frequency signal.

2.3. PSK Modulator

Figure 8 shows the configuration of the PSK modulator, which consists of a microstrip line, slot line, and two PIN diodes mounted on a half-wavelength slot ring [18]. The half-wavelength slot ring creates two equal quarter-wavelength paths, upper and lower, for the input signal to reach the output port. Two PIN diodes D1 and D2 are mounted on the slot ring in anti-parallel arrangement to control the two paths. The diodes D1 and D2 can be controlled using the bias polarity applied to the inner conductor of the slot ring. When the diode D1 is ON (short), the quarter-wavelength upper slot line and quarter-wavelength extended microstrip line create a low-loss microstrip-to-slot transition, and the input signal propagates through the lower half of the slot ring. In contrast, the signal propagates through the upper half if the diode D2 is ON (short). Thus, the phase of the signal can be altered between 0° and 180° based on the diode's bias condition.

Figure 9 shows the simulated phase of S_{21} of the PSK modulator. At 14.71 GHz, the simulated phase difference is found with 180° between the two conditions, diode D1 and D2 ON. Thus, the simulated results confirm the phase switching operation of the proposed PSK modulator.

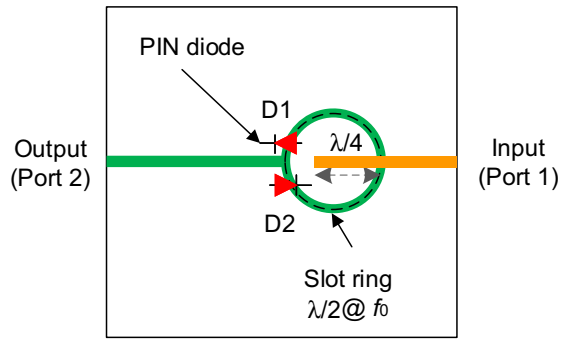

Figure 8. Structure of the PSK modulator.

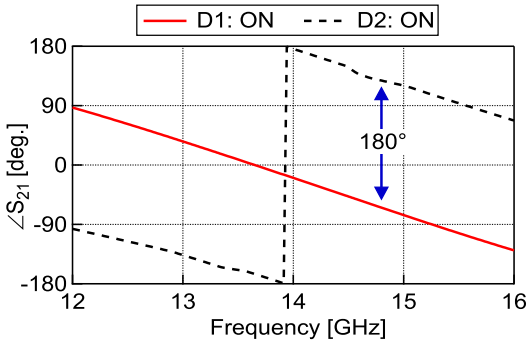

Figure 9. Simulated phase of S_{21} of the PSK modulator.

2.4. Bandstop Filter

Figure 10 shows the bandstop filter used in this study, which is based on two quarter-wavelength ($\lambda/4$) open stub resonators. The purpose of this bandstop filter is to improve the elimination of the fundamental frequency (f_0) signal of the Push-Push oscillator. The two open stub resonators resonate at two different frequencies centering at f_0 to produce a high and wider stopband. These stubs are separated by an arbitrary microstrip line, A. The length of A defines the passband. The mathematical model of this bandstop filter is briefly explained in [22].

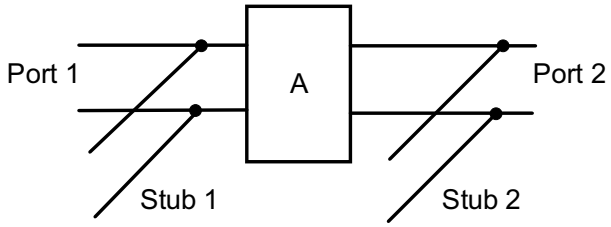

Figure 10. Equivalent circuit of the bandstop filter used in the proposed AIAA.

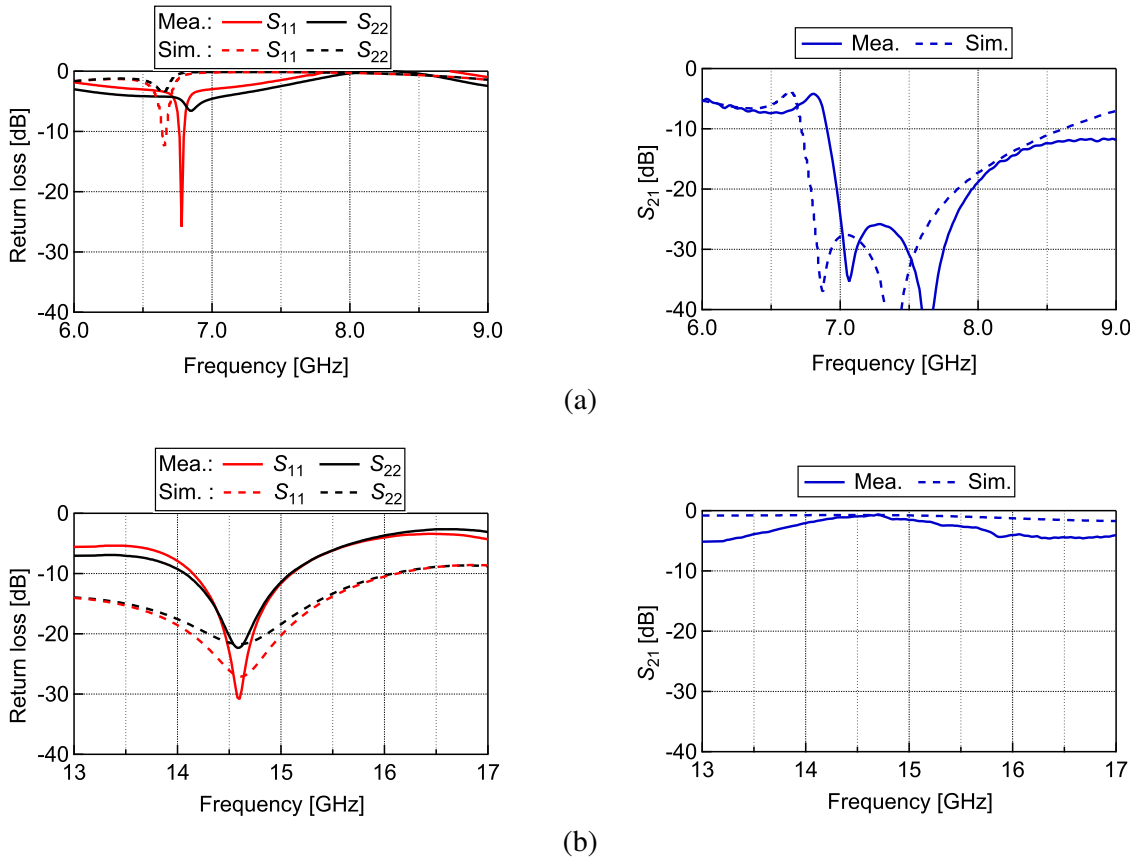

Figure 11. Simulated and measured results of the bandstop filter. (a) Stop-band. (b) Pass-band.

Figure 11 presents the simulated and measured stop- and pass-bands of the bandstop filter. More than 25-dB signal rejection is achieved at 7.35 GHz (f_0) in the measurement. The return loss (S_{11}, S_{22}) is better than 19 dB, and the insertion loss (S_{21}) is just 0.62 dB at 14.7 GHz ($2f_o$) as shown in Fig. 11. The measured results roughly agree well with the simulated ones.

2.5. Operating Principle of Proposed Antenna

Figure 12 shows the operational mechanism of the proposed AIAA. The RF power from the Push-Push oscillator excites the antenna elements #1, #2 and #3, #4 through the MSL-SL transition and PSK modulator, respectively. As the PSK modulator can switch the phase of the fed signal of the antenna elements #3 and #4, the antenna can produce dual beams. As shown in Fig. 12, the sum radiation pattern is generated when diode D1 is ON. In contrast, the antenna exhibits difference radiation pattern for the ON condition of diode D2 in the $\phi = 0^\circ$ plane.

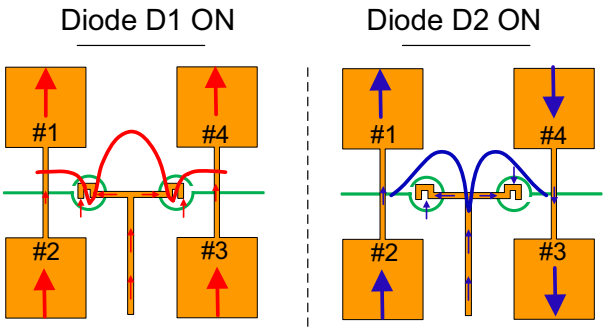

Figure 12. Phase relations on the antenna elements.

2.6. AIAA Design

Figure 13 shows photographs of the Ku-band prototype antenna with top and bottom views. The antenna is designed using Momentum of Keysight Technologies' Advanced Design System (ADS). The proposed AIAA is fabricated on a polytetrafluoroethylene (PTFE) substrate with a dielectric constant of 2.15 and thickness of 0.8 mm. Antenna elements and HEMTs are mounted on the top side, whereas the PSK modulator is placed on the backside of the substrate. The size of the prototype is 40 mm × 70 mm.

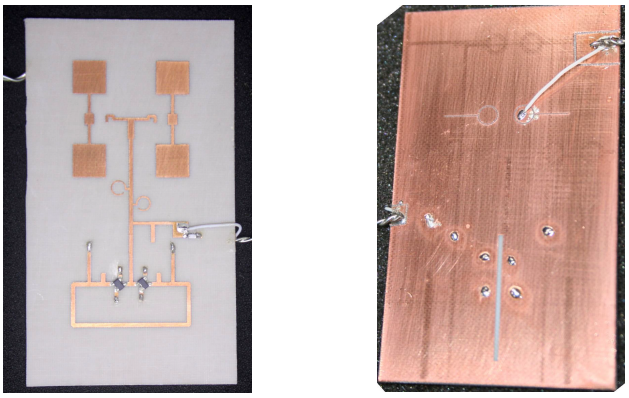

Figure 13. Fabricated prototype of the proposed Ku-band beam switchable AIAA (40 mm × 70 mm). (a) Top view. (b) Bottom view.

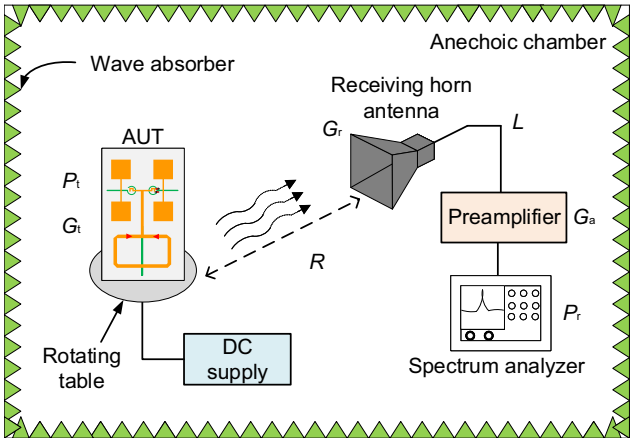

Figure 14. Measurement setup to investigate the proposed AIAA.

3. MEASURED RESULTS

3.1. Measurement Setup

Figure 14 shows the measurement setup used for this study. A spectrum analyzer (Agilent E4407B) and double ridged waveguide horn antenna (TR17206, Model no. 3115 by EMC Test Systems) are used

for this setup. The radiated radio waves from the proposed AIAA were measured across the receiving horn antenna ($G_r = 13.2\,\text{dBi}$) using the spectrum analyzer. To compensate the loss of a long cable ($L = 6.6\,\text{dB}$) as well as to increase the received power sensitivity, a pre-amplifier (Hewlett Packard 8449B) of $G_a = 30\,\text{dB}$ was used. The distance between the proposed AIAA and the horn antenna is kept at 1.3 m ($R \gg \frac{2D^2}{\lambda}$, where D denotes the dimension of the antenna) to ensure the far-field region.

3.2. Radiated Power, Stability, and FOM

Figure 15 highlights the received power and stability of the proposed AIAA for ideal short conditions instead of the diode D1 (accounts for sum pattern) to illuminate the ideal performance in the measurement. The free-running oscillation frequency was 14.7 GHz, close to the standalone Push-Push oscillator prototype. The suppression of the fundamental frequency signal is around 29.5 dB. As shown in Fig. 15(a), the maximum received power (P_r) was $-2.5\,\text{dBm}$ obtained at 4.1-V, 280-mA bias condition where cable loss and preamplifier gain are included. The effective isotropic radiated power (EIRP) is evaluated using Friis equation:

$$\text{EIRP}\,[\text{dBm}] = P_t + G_t = P_r - G_r + L - G_a + 20\log_{10}\left(\frac{4\pi R}{\lambda}\right). \tag{6}$$

The EIRP of the proposed AIAA becomes +18.97 dBm using Eq. (6). To find out the transmitted power (P_t), gain (G_t) of the passive antenna is required. Since the passive antenna gain (G_t) is 10.9 dBi in simulation, the radiated power (P_t) in the measurement is calculated as +8.07 dBm, which agrees well with the standalone oscillator prototype. By dividing the transmitted power (P_t) to the input DC power yields a DC-to-RF conversion efficiency of around 0.56%. The conversion efficiency is low because the proposed AIAA employs a second-harmonic oscillator based on the Push-Push principle.

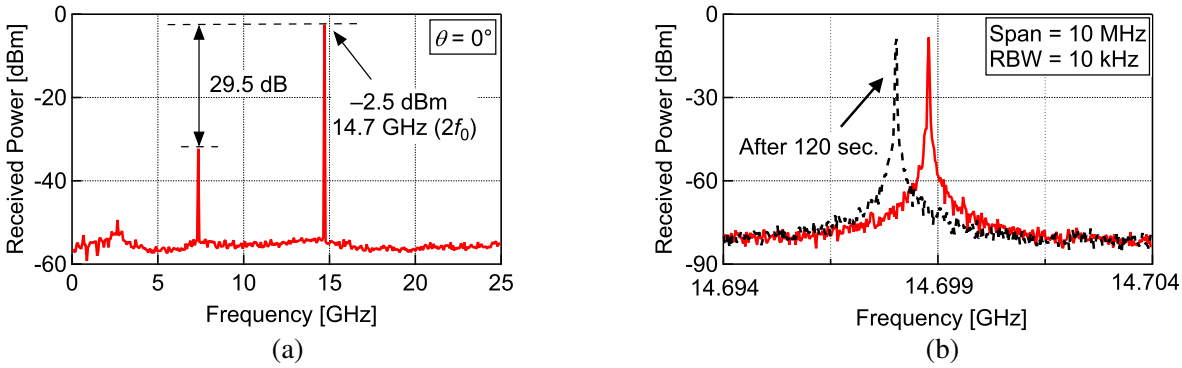

Figure 15. Measured performance of the developed AIAA prototype. (a) Received power for ideal condition at 4.1-V, 280-mA bias condition including cable loss and preamplifier gain. (b) Stability plot (Span = 10 MHz, RBW = 10 kHz, and VBW = 10 kHz).

Figure 15(b) shows the frequency stability plot of the proposed AIAA. As the proposed AIAA is integrated with a free-running oscillator, oscillation frequency shifting occurs with time. Thus, frequency stability is an important objective for the oscillating type AIAA. Fig. 15(b) indicates 800 kHz of frequency shifting over 120-seconds span of time.

The phase noise was found to be $-105.3\,\text{dBc/Hz}$ at 1-MHz offset from the oscillation frequency. The performance of the oscillator can be measured using a common figure of merit (FOM), which can be calculated by

$$\text{FOM} = L(\Delta f) - 20\log_{10}\left(\frac{f_0}{\Delta f}\right) + 10\log_{10}\left(\frac{P_{\text{DC}}}{1\,\text{mW}}\right). \tag{7}$$

Using Eq. (7), the FOM of the Push-Push oscillator of this proposed AIAA at 1-MHz offset frequency is $-158.05\,\text{dBc/Hz}$, where $L(\Delta f)$ is the phase noise, f_0 the oscillation frequency, and P_{DC} the DC power consumption.

3.3. Received Power Using PIN Diodes

Figure 16 shows the maximum received output powers for diode D1 and D2 ON conditions. Two PIN diodes (DSG9500-000 by Skyworks) are used for the PSK modulator. To turn on diodes D1 and D2, positive (+0.9 V, 10 mA) and negative (−1.0 V, 10 mA) switching voltages were applied to the inner conductor of the slot ring of the PSK modulator. From Fig. 16(a), we can note that around 1.2-dB lower output power is observed compared to Fig. 15(a) and can be referred to as diode loss. The unwanted fundamental frequency signal (f_0) at 7.35 GHz is 21.7 dB lower than the oscillation frequency ($2f_0$) at 14.7 GHz. By using Eq. (6), the EIRP and transmitted power of the sum pattern become +17.8 dBm and +6.87 dBm, respectively.

In the case of diode D2 ON condition, the maximum received power is obtained around −5.1 dBm at $\theta = -30°$. Considering 9.4 dBi simulated antenna gain, the EIRP and transmitted power are calculated as +16.37 dBm and +6.97 dBm, respectively. In this case, the fundamental signal suppression is 17.1 dB. Although a significant decrease of unwanted signal suppression is detected compared to Fig. 15(a), no significant spurs or frequency jumping were observed during the measurement. The difference between Figs. 16(a) and (b) is due to the gain difference between the sum and difference radiation patterns. The measured phase noise was the same as the above mentioned phase noise for both of these conditions.

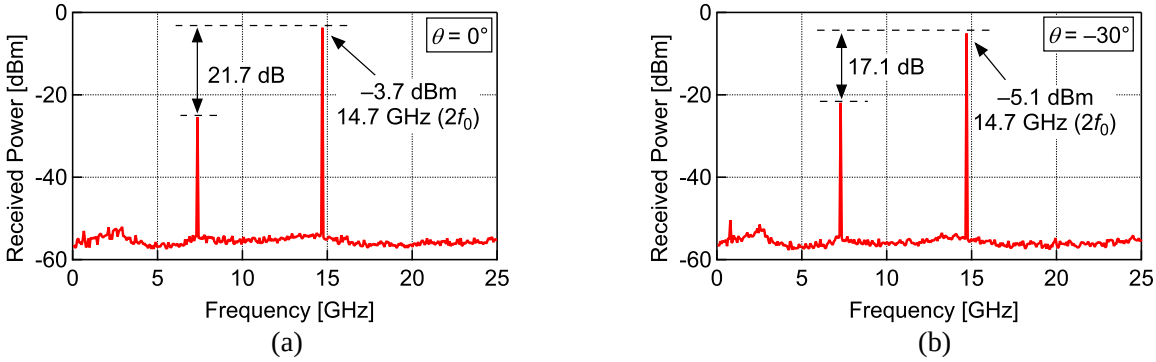

Figure 16. Measured received power with PIN diodes. (a) Diode D1: ON. (b) Diode D2: ON.

3.4. Radiation Pattern Measurements

Figure 17 shows the switching of the radiation patterns of the proposed AIAA in the $\phi = 0°$ plane. The received power at the spectrum analyzer was recorded by rotating the proposed AIAA from −180° to +180°. The received power is then normalized to its maximum value to find out a rational relationship with the simulated results. Here, the red and black lines represent the co- and cross-polarizations, respectively. The measured radiation patterns of the proposed AIAA and a separately designed passive antenna are compared with the simulated passive antenna's radiation pattern. The antenna exhibits a sum radiation pattern as shown in Fig. 17(a), when diode D1 is ON. In contrast, Fig. 17(b) shows the difference radiation pattern for diode D2 in ON condition. Thus, the concept for the beam switching between the sum and difference radiation patterns is found feasible in both simulation and measurements. As shown in Figs. 17(a) and (b), the measured cross-polarization levels of the AIAA were around 16 dB and 12 dB lower than the maximum co-polarization patterns for the AIAA and 17.1 dB and 17.9 dB for the passive antenna, respectively. The correlation between the measurement and simulation is noteworthy because they follow a similar trend. In the measurement, the radiation patterns of the proposed AIAA are found similar to the passive antenna's radiation patterns after covering the Push-Push oscillator by wave absorber. Thus, the discrepancy between the measured AIAA and the passive antenna can be attributed to the radiation from the oscillator.

3.5. Results Summery and Performance Comparison

Table 1 shows the performance summary of the proposed AIAA. The beam state can be switched by the diode conditions of D1 and D2. Almost equal transmitted power with around 0.42% DC-to-RF efficiency

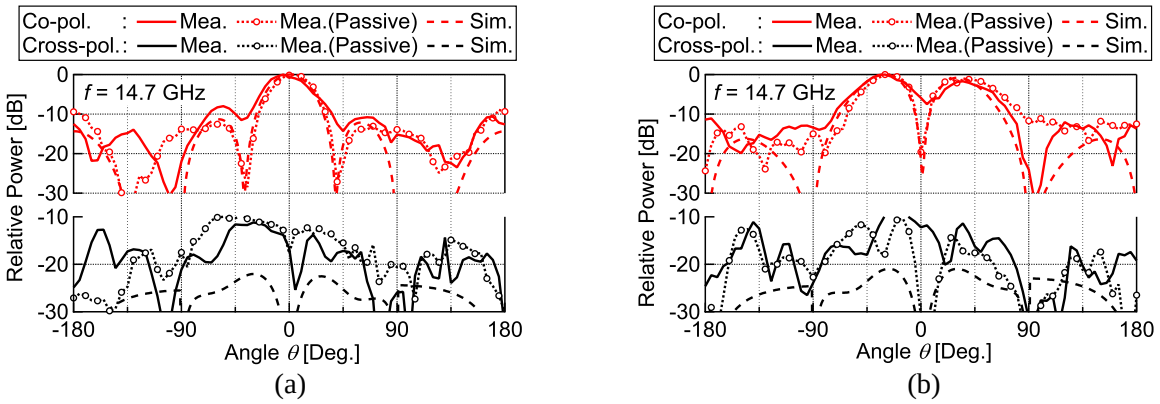

Figure 17. Measured and simulated radiation patterns. (a) Diode D1: ON. (b) Diode D2: ON.

at the same oscillation frequency is observed for both the states. The EIRP difference between the beam states is due to the gain difference at $\theta = 0°$ and $-30°$.

Table 2 shows the performance comparison with those in literature. In most of the cases, direct integration of active devices with the radiator has been applied with various techniques to switch/steer

Table 1. Performance summary of the prototype AIAA.

Diode condition		Beam state	Measured freq. [GHz]	EIRP [dBm]	Transmitted power (P_t) [dBm]	DC-to-RF efficiency [%]
D1	D2					
ON	OFF	Sum	14.7	+17.77	+6.87	0.424
OFF	ON	Difference	14.7	+16.37	+6.97	0.434

Table 2. Performance comparisons between the published beam steering/switchable self-oscillating AIAs.

Ref.	Freq. [GHz]	Reconfigurable type	Technique	Active device	No. of active elements	FOM [dBc/Hz]	EIRP [dBm]
[7]	9.54	Switching	RF signal combination	Gunn diode	1	NA†	+15.98
[8]	4.6	Steering	PIN diodes with radiators	HJFET	1	−162.6*	+5.4 to +9.3
[9]	5	Steering	Switched-line phase shifter	HJFET	1	−161.1*	+9.14 to +12.96
[12]	12.45	Switching	Mode switching	Gunn and MESFET	2	NA†	+14
[13]	6.2	Switching	Injection locking	MESFET	4	NA†	+30
[14]	5.2	Switching	RF signal combination	HJFET	1	−167.2*	+14.87
This Work	**14.7**	**Switching**	**RF signal combination**	**HEMT**	**2**	**−158.05**	**+17.77**

* Calculated from given value, † NA: Not reported in literature.

the beam of the self-oscillating type AIAA. Integrating with the Push-Push oscillator, this study shows an extension of frequency range of the active devices. Overall, very good EIRP and switching performances have been obtained form the proposed prototype AIAA.

4. CONCLUSION

A dual-beam switchable self-oscillating AIAA has been proposed for Ku-band wireless power transfer systems. The proposed AIAA can also be used for wireless communications by incorporating a modulation mechanism like PSK, FSK, and ASK. The concept is experimentally examined using a prototype antenna. The demonstration of the beam switching and the extension of the frequency range were successfully confirmed. This design layout can be easily extended to achieve dual-axis dual-beam switchable AIAAs by inclining the antenna elements to $\pm 45^{\circ}$.

ACKNOWLEDGMENT

The authors would like to acknowledge the invaluable help from Mr. Kouki Tokumaru, a former master student of Saga University for the fabrication of the Push-Push oscillator prototype used in this work. This work was made possible from a grant by JSPS KAKENHI Grant Number JP17K06429.

REFERENCES

1. Chang, K., R. A. York, P. S. Hall, and T. Itoh, "Active integrated antennas," *IEEE Trans. Microw. Theory Techn.*, Vol. 50, No. 3, 937–944, 2002.
2. Qian, Y. and T. Itoh, "Progress in active integrated antennas and their applications," *IEEE Trans. Microw. Theory Techn.*, Vol. 46, No. 11, 1891–1900, 1998.
3. Toyoda, I., Y. Furukawa, E. Nishiyama, T. Tanaka, and M. Aikawa, "Polarization agile self-oscillating active integrated antenna for spatial modulation wireless communications," *Electron Comm. Jpn.*, Vol. 101, No. 11, 37–44, 2018.
4. Hasan, M., E. Nishiyama, and I. Toyoda, "A polarization switchable active integrated array antenna with a single-lambda slot-ring Gunn oscillator and PSK modulator," *IEICE Comm. Express*, Vol. 8, No. 12, 560–565, 2019.
5. Hasan, M., H. Ushiroda, E. Nishiyama, and I. Toyoda, "A polarization switchable active array antenna integrating a multiport oscillator and PSK modulators," *Proc. 2018 Asia-Pacific Microw. Conf. (APMC 2018)*, 1253–1255, Kyoto, Japan, 2018.
6. Hasan, M., E. Nishiyama, and I. Toyoda, "A microstrip-line Gunn oscillator loaded active integrated array antenna using inclined patches for polarization switching function," *Proc. 2020 Int. Symp. Antennas Propag. (ISAP 2020)*, 797–798, Osaka, Japan (Virtual), 2021.
7. Hasan, M., E. Nishiyama, and I. Toyoda, "A beam switchable self-oscillating active integrated array antenna using Gunn oscillator and magic-Ts," *IEICE Trans. Commun.*, Vol. E104-B, No. 11, 2021.
8. Wu, C. and T. Ma, "Pattern-reconfigurable self-oscillating active integrated antenna with frequency agility," *IEEE Trans. Antennas Propag.*, Vol. 62, No. 12, 5992–5999, 2014.
9. Singh, R. K., A. Basu, and S. K. Koul, "A novel pattern-reconfigurable oscillating active integrated antenna," *IEEE Antennas Wirel. Propag. Lett.*, Vol. 16, 3220–3223, 2017.
10. Xiao, S., Z. Shao, and M. Fujise, "Pattern reconfigurable millimeter wave microstrip quasi-Yagi active antenna," *Proc. 2005 Asia-Pacific Microw. Conf. (APMC 2005)*, Suzhou, China, 2005.
11. Liu, Z., Y. Chang, and T. Ma, "High-efficiency self-oscillating active integrated antenna using metamaterial resonators and its application to multicarrier radio frequency identification systems," *IEEE Trans. Antennas Propag.*, Vol. 64, No. 9, 3803–3810, 2016.
12. Minegishi, M., J. Lin, T. Itoh, and S. Kawasaki, "Control of mode-switching in an active antenna using MESFET," *IEEE Trans. Microw. Theory Techn.*, Vol. 43, No. 8, 1869–1874, 1995.

13. Chew, S. T. and T. Itoh, "A 2×2 beam-switching active antenna array," *Proc. 1995 IEEE MTT-S Int. Microw. Symp. Dig. (IMS 1995)*, Vol. 2, 925–928, Orlando, FL, USA, 1995.
14. Singh, R. K., A. Basu, and S. K. Koul, "Reconfigurable oscillating active integrated antenna using two-element patch array for beam switching applications," *Engineering Reports*, Vol. 1, No. 7, e12071, 2019.
15. Lin, J., T. Itoh, and S. Nogi, "Mode switch in a two-element active array," *1993 IEEE Antennas Propag. Soc. and Int. Symp. Dig. (AP-S 1993)*, 664–667, Ann Arbor, MI, USA, 1993.
16. Hasan, M., E. Nishiyama, T. Tanaka, and I. Toyoda, "Design of dual-beam switchable self-oscillating active array antenna integrating positive feedback type Push-Push oscillator and PSK modulator," *Proc. 2020 Int. Conf. Emerg. Tech. for Comm. (ICETC 2020)*, A4–A5, Japan (Virtual), 2020.
17. Lin, Y. and T. Ma, "Frequency-reconfigurable self-oscillating active antenna with gap-loaded ring radiator," *IEEE Antennas Wirel. Propag. Lett.*, Vol. 12, 337–340, 2013.
18. Tanaka, T., H. Otani, and M. Aikawa, "Microwave transmitter module integrating slot array antenna, Push-Push oscillator and PSK modulator," *Proc. 2010 Asia-Pacific Microw. Conf. (APMC 2010)*, 1023–1026, Yokohama, Japan, 2010.
19. Lima, E., T. Tanaka, and I. Toyoda, "A novel low phase noise Push-Push oscillator employing dual-feedback sub-oscillators," *Progress In Electromagnetics Research M*, Vol. 75, 141–148, 2018.
20. Dong, Y. and T. Itoh, "Planar ultra-wideband antennas in Ku- and K-band for pattern or polarization diversity applications," *IEEE Trans. Antennas Propag.*, Vol. 60, No. 6, 2886–2895, 2012.
21. Kawahata, K., T. Tanaka, and M. Aikawa, "A K-band Push-Push oscillator with high suppression of undesired harmonic signals," *IEICE Trans. Electron.*, Vol. E86-C, No. 8, 1433–1437, 2003.
22. Shairi, N. A., B. H. Ahmad, and P. W. Wong, "Bandstop to allpass reconfigurable filter technique in SPDT switch design," *Progress In Electromagnetics Research C*, Vol. 39, 265–277, 2013.
23. Balanis, C. A., *Antenna Theory: Analysis and Design*, 3rd Edition, John Wiley, Hoboken, NJ, 2005.